MTLA 41 (2025) 102433

Contents lists available at ScienceDirect

Materialia

journal homepage: www.elsevier.com/locate/mtla

Microstructure and mechanical performance of AISI D2 tool steel after standard and modified deep cryogenic treatment

Venu Yarasu [a,*], Bojan Podgornik [a], Barbara Setina Batic [a], Marko Sedlacek [a], Črtomir Donik [a], Francisco Ruiz-Zepeda [a,b]

[a] Institute of Metals and Technology, Lepi pot 11, SI-1000, Ljubljana, Slovenia
[b] Department of Materials Chemistry, National Institute of Chemistry, Hajdrihova 19, SI-1000, Ljubljana, Slovenia

ARTICLE INFO

Keywords:
Steel
Isothermal heat treatments;Cyclic response
Martensite
Fracture toughness

ABSTRACT

This research investigates the potential benefits of cyclic deep cryogenic treatment (CDCT) on AISI D2 cold-work tool steel, focusing on hardness and fracture toughness enhancement and their correlation with structural changes. While conventional deep cryogenic treatment (DCT) at −196 °C has demonstrated positive effects on tool steel properties, the specific long durations of DCT remain a limitation for industrial applications. AISI D2 steel specimens underwent conventional heat treatment and deep cryogenic treatment (DCT) at −196 °C for 24 hours, alongside CDCT with 2, 5, and 10 cycles within the same temperature range. The microstructural evolution, phase transformations, residual stresses, hardness, and fracture toughness induced by these treatments were thoroughly analyzed using advanced characterization techniques, including SEM-EDS, EBSD, XRD, and TEM. Macro- and micro-hardness measurements were conducted using Rockwell and Vickers methods, while fracture toughness was assessed using circumferentially notched and fatigue-pre-cracked tensile bar specimens. The results indicate that all samples exhibited comparable bulk hardness values. However, fracture toughness showed significant enhancement with CDCT, with the CDCT2 treatment achieving the highest improvement—68 % greater than that of the conventional treatment. Microstructural analysis reveals refined martensitic structures with nanotwins, stacking faults, dislocations, an enhanced count of small secondary carbides, increased precipitation of nanosized carbides, and lower residual stresses as key contributors to the enhanced mechanical properties.

1. Introduction

Tool steels play a pivotal role in various industrial applications, serving as essential materials for the production of cutting tools, molds, dies, and other components subjected to harsh operating conditions [1–4]. Among the various categories of tool steels, cold-work tool steels occupy a central position due to their versatility and cost-effectiveness in meeting the demands of modern manufacturing industries [5–7]. However, despite their inherent advantages, the continuous evolution of manufacturing technologies in sectors such as aerospace, automotive, and energy has heightened the demand for tool steels with enhanced properties to prolong tool life and improve productivity [3,8,9].

The mechanical properties of tool steels, particularly hardness and fracture toughness, play a pivotal role in determining their suitability for specific applications [10,11]. Hardness influences the material's resistance to wear and plastic deformation, which is crucial for maintaining sharp cutting edges and withstanding abrasive forces during operation. Conversely, fracture toughness dictates the material's ability to resist crack propagation and withstand sudden impact loads, essential for preventing fatigue, premature failure and ensuring tool longevity.

To optimize the mechanical properties of tool steels and meet the evolving demands of industrial applications, various processing techniques, including heat treatment and surface treatments, are employed [12–17]. Among these techniques, cryogenic treatments have garnered significant attention for their ability to refine microstructure, enhance hardness, and improve overall mechanical properties [18,19]. Deep cryogenic treatment (DCT), in particular, has emerged as a promising approach by subjecting tool steels to ultra-low temperatures (–196 °C) to induce beneficial microstructural transformations and improve wear resistance. For instance, Essam et al. [20,21] studied the effect of deep cryogenic treatment (DCT) on microstructure, hardness, and wear behavior of various cold-work and shock resistant steels. They

* Corresponding author.
E-mail address: venu.yarasu@imt.si (V. Yarasu).

https://doi.org/10.1016/j.mtla.2025.102433
Received 13 January 2025; Accepted 12 May 2025
Available online 21 May 2025

concluded that the DCT refines the microstructure and enhances the hardness and thereby improves wear resistance. Numerous previous studies have demonstrated notable improvements in surface properties and wear resistance of tool steels following DCT [20–28], highlighting its potential as a viable enhancement technique. However, traditional DCT treatments often require prolonged durations, ranging from several hours to days, depending on the material and desired properties. For instance, Das et al. studied the effect of DCT duration on the properties of D2 cold-work tool steel, identifying 36 hours as the optimal duration to achieve desirable material properties (maximum wear resistance) [22]. Similarly, Jurci et al. reported that 17 hours of DCT was beneficial for Vanadis 6 cold-work tool steel [23], while Xu et al. found that DCT beyond 5 hours did not further affect the microstructure and mechanical properties of AISI M35 high-speed steel [24]. These studies indicate that DCT involves longer durations for cold-work tool steels, and the treatment duration depends on the material composition and heat treatment process parameters. This extended processing time for DCT involving treatments, although reducing the need for double or triple tempering, can be a significant bottleneck in industrial applications.

In recent years, there has been growing interest in exploring the potential benefits of cyclic cryogenic treatment (CCT) as a novel approach to further optimize the properties of materials including composites [25], high-entropy alloys [29], bulk-metallic glasses [30], aluminum [31] and steel [24,25] alloys. CCT treatment emerges as a promising alternative approach that offers the potential to achieve similar or even superior improvements in properties with shorter processing times. The repeated exposure to cryogenic temperatures in CCT is hypothesized to induce more pronounced microstructural refinements compared to a single DCT cycle. This could potentially lead to enhanced hardness, fracture toughness, and overall mechanical performance of tool steels [32,33]. For example, a recent study conducted by Chen et al. investigated the effect of cyclic cryogenic treatment (CCT) on the performance of 51CrV4 spring steel [34]. Their findings revealed significant enhancements in mechanical properties, with CCT resulting in about 15 % increase in yield and tensile strength, a 4 % increase in impact toughness, and about 43 % reduction in wear loss. Statistical analysis further identified the number of cycles and holding time as critical process parameters influencing the impact toughness of 51CrV4 spring steel. Moreover, CCT treatment has great potential to reduce the extended process duration required for DCT while improving material properties. However, despite its potential, the specific effects of cyclic cryogenic treatment on tool steel properties, particularly its influence on microstructural evolution and mechanical behavior, remain relatively unexplored.

This study aims to address this research gap by investigating the impact of cyclic deep cryogenic treatment (CDCT) on the microstructure and properties of AISI D2 cold-work tool steel. Unlike conventional deep cryogenic treatment (DCT), which often demands extended durations to achieve optimal performance, CDCT introduces controlled thermal cycling that could enhance material properties in a more time-efficient manner. This study is the first to comprehensively evaluate the effects of CDCT on both hardness and fracture toughness, shedding light on the underlying mechanisms responsible for these improvements. By comparing CDCT with conventional heat treatment and DCT, this research provides valuable insights into the correlation between cyclic thermal exposure, phase transformation, carbide precipitation, and mechanical performance. The objectives of the study are twofold: first, to exploit the fracture toughness of D2 steel treated with CDCT, and second, to explore the beneficial effects of CDCT over conventional and deep cryogenic treatment, particularly regarding achieving improved properties with shorter treatment durations. The ultimate goal is to establish CDCT as a viable alternative that not only enhances the mechanical performance but also mitigates the time limitations of conventional deep cryogenic treatments in industrial applications. The findings from this study could pave the way for optimizing cryogenic processing strategies, leading to improved performance and durability of tool steels used in demanding engineering applications.

2. Material and methods

2.1. Material

The material used in this study was commercially available AISI D2 steel, supplied in the hot rolled and soft-annealed condition. The verified chemical composition of selected steel in mass fraction is given in Table 1.

2.2. Methods

Circumferentially notched tensile samples with dimensions as shown in Fig. 1 were prepared from rolled bars using CNC machining. Subsequently, these samples underwent fatigue pre-cracking under rotational bending at 65N−70 N for 5 min, resulting in a pre-crack length of 0.4 mm in the V-notch [35]. The Circumferentially Notched and Fatigue Pre-Cracked Tensile Bar specimens (CNPTB) were then subjected to hardening at 1000 °C for 30 min and quenched in a single step using a horizontal vacuum furnace with uniform high-pressure nitrogen gas quenching at 5 bar pressure. The hardening treatment included preheating, austenitizing, and quenching. Preheating was conducted at temperatures of 650 °C and 850 °C for 10 min to achieve uniform temperature distribution between the surface and core, minimizing thermal distortion.

Following hardening, the samples were divided into three batches for subsequent treatments. The first batch underwent double tempering at 570 °C for 2 hours and was denoted as conventionally heat treated (CHT). The second batch was subjected to deep cryogenic treatment (DCT) for 24 hours, denoted as DCT24, through controlled immersion in liquid nitrogen. After DCT24, these samples underwent double tempering. The final batch underwent cyclic deep cryogenic treatment (CDCT), a modified DCT process involving multiple cycles of exposure to liquid nitrogen and bringing samples back to room temperature. Cooling and heating rates were ~2.5 °C/s and ~0.2 °C/s, respectively. The samples were subjected to CDCT at three different conditions: CDCT2 (2 cycles of DCT), CDCT5 (5 cycles of DCT), and CDCT10 (10 cycles of DCT). A detailed schematic representation of the heat treatment methods is provided in Fig. 2. The process parameters for hardening were selected based on ASM recommendations [36]. It is well established that, under conventional tempering conditions (typically between 200 °C and 550 °C), D2 tool steel can exhibit hardness values in the range of 50–60 HRC [22,36]. However, the tempering parameters in our study were intentionally chosen to exceed 550 °C. This decision was driven by our primary objective of exploring fracture toughness rather than maximizing hardness.

Microstructural characterization of the CNPTB specimens following CHT, DCT, and CDCT treatment involved standard metallographic preparation. Specimens were sectioned, polished, and examined using advanced characterization techniques, including scanning electron microscopy (SEM), energy dispersive spectroscopy (EDS), electron backscattered diffraction (EBSD), x-ray diffraction (XRD), and transmission electron microscopy (TEM). A JEOL 6500F SEM equipped with an INCA EDS system (IMT) was employed for SEM-EDS analysis. EBSD analysis was conducted using a ZEISS Crossbeam 550 FIB-SEM Gemini II. EBSD mapping was performed under vacuum conditions below 10^{-6} mbar, with an accelerating voltage of 20 kV, a beam current of approximately 10 nA, a scan area of 43 × 33 μm^2, and a step size of 0.04 μm. EBSD data, processed using OIM software (AMETEK, Mahwah, NJ, USA), was used

Table 1
Chemical composition of AISI D2 steel in wt.%.

C	Mn	Si	S	P	Cr	Mo	V	Fe
1.5	0.29	0.4	<0.01	<0.01	11.1	0.79	0.72	Bal.

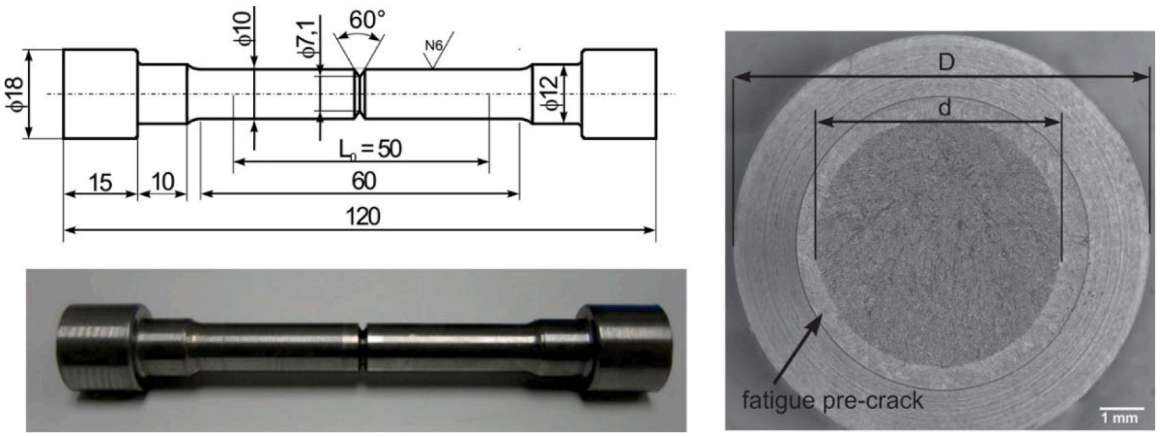

Fig. 1. Dimensions of Circumferentially Notched and Fatigue Pre-Cracked Tensile Bar specimens (CNPTB).

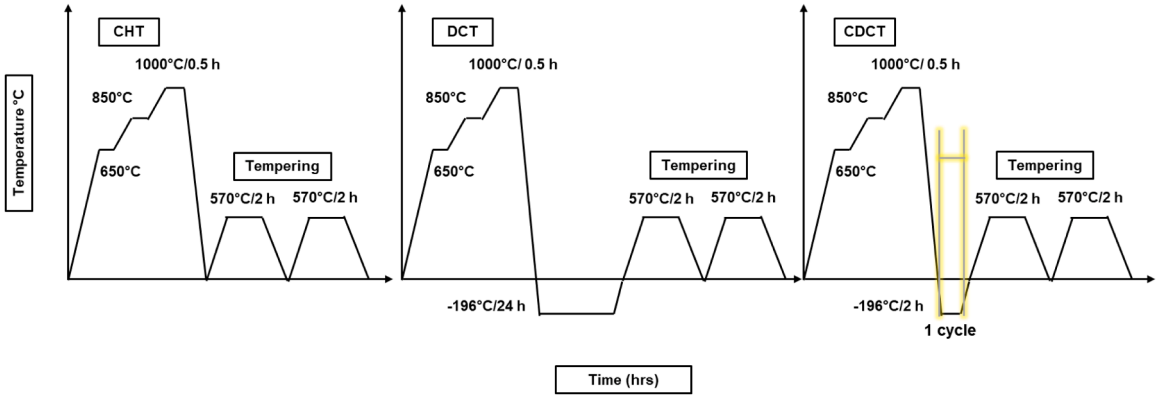

Fig. 2. Schematic diagram for the heat treatment cycles used for AISI D2 steel.

to identify phase variations among the CHT, DCT, and CDCT samples.

Quantification of carbides was conducted on twenty randomly acquired backscattered SEM images at 3000X magnification using Image J software. Phase analysis was conducted using both EBSD, presented as inverse pole figure (IPF) maps, and X-ray diffraction (XRD). XRD analysis was performed using a PANalytical XPert Pro diffractometer (Cu Kα radiation) over a 2θ range of 30–100°, with a step size of 0.02°and a dwell time of 45 s. TEM was employed to investigate nanoscale microstructural features. TEM lamellae were prepared using the ZEISS Crossbeam 550 FEB-SEM Gemini II (IMT) and analyzed using a Thermo Fisher TEM operated at 200 kV.

For hardness and fracture toughness measurements, CNPTB specimens were utilized, following the procedures detailed in Ref. [35]. Rockwell hardness measurements were conducted on the circumferential surface (ϖ12) of both fractured parts of the CNPTB specimen using a Wilson Rockwell B 2000 machine, in accordance with ISO 6508–1:2016 standard protocols. Microhardness measurements (HV0.1) were conducted on the metallographic samples in accordance with ISO 6507–1:2018 standard procedures. The mean Rockwell and Vickers hardness value and standard deviation were calculated and reported for each sample. Fracture toughness was assessed utilizing the fatigue pre-cracked specimens in accordance with the plain strain model [37]. A minimum of nine identically conducted tests were averaged to measure the fracture toughness (K_{1C}). Tensile loading until fracture was carried out at room temperature using an Instron 1255 tensile test machine with a crosshead speed of 1.0 mm/min. Subsequently, the size of brittle fractured area was measured to determine fracture toughness.

Fracture toughness was calculated using Eq. (1), which is valid for linear elastic behavior, as confirmed for all the specimens tested:

$$K_{1C} = \frac{P}{D^{3/2}}\left(-1.27 + 1.72\left(\frac{D}{d}\right)\right) \quad (1)$$

Where P represents the load at fracture, D denotes the outside diameter of the non-notched section (10 mm), and d signifies the diameter of the brittle fractured area. Nine specimens were prepared for each test group, and the diameter of the brittle fractured area was measured for each specimen.

Residual stress measurements were performed using the incremental hole-drilling method (IHD) according to ASTM E837–20. A Sint Technology RESTAN MTS 3000 system, equipped with a high-speed air turbine (20,000–400,000 rpm), was employed for this purpose. Strain evolution during the IHD process was monitored using HBM type B counterclockwise strain gauge rosettes. A diamond-coated inverted cone end mill (1.6 mm nominal diameter, resulting in a final hole diameter of 1.80 mm) was used for drilling. Twenty linearly distributed drilling steps, each with a depth of 0.02 mm (total drilling depth: 0.3 mm), were performed. Strain data was acquired using an RSM Data Acquisition system (version 7.5). Non-uniform stress profiles were then calculated using the integral method within EVAL software (version 8.01).

3. Results and discussion

3.1. Microstructure

SEM imaging coupled with energy dispersive X-ray spectroscopy (EDS) and electron backscattered diffraction (EBSD) measurements were performed in order to gain qualitative and quantitative information about the phase distribution and morphology of the samples. Fig. 3

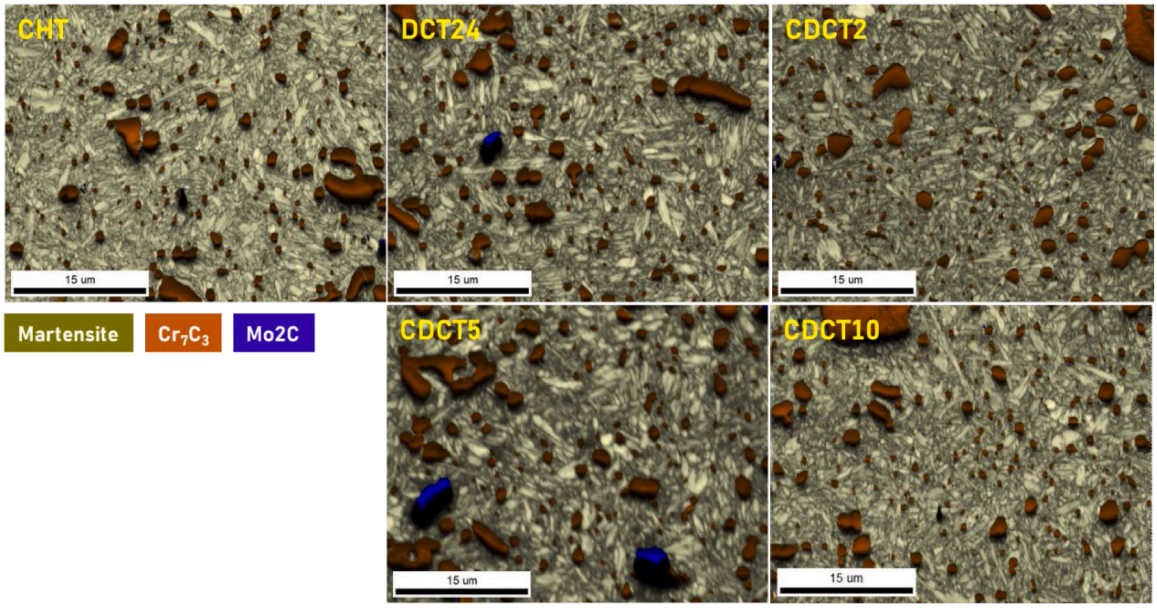

Fig. 3. EBSD IQ Microstructure and Phase maps of AISI D2 steel after different heat treatments.

presents the representative SEM and EBSD IQ microstructures and phase maps of CHT, DCT24, and CDCT specimens after double tempering.

All microstructures comprise tempered martensite and carbides of varying sizes, with no retained austenite observed in any of the treated samples. The microstructures primarily feature three sizes of carbides: primary carbides, secondary carbides, and small secondary carbides in the nanometer range. The primary carbides, with sizes above 5 μm, are predominantly chromium-rich carbides (M_7C_3), where M represents elements such as Cr, V, Mo, and Fe. Secondary carbides, ranging from 1 to 5 μm, also exhibit similar composition and distribution within the microstructure, as shown in Fig. 4, a representative sample (CHT) electron microscope image with corresponding elemental maps. The nature of these carbide particles and classifications in AISI D2 steel were also reported recently by several research groups [38,39]. The visual inspection of the EBSD images revealed that the martensite laths in DCT and CDCT samples appear to be finer compared to those in the CHT samples. Additionally, these CDCT treatments enhanced the number of small secondary carbides (SSCs) with diameter <1 μm and reduced the overall size distribution of small carbides. Furthermore, the distribution of SSCs within the matrix exhibited a more homogeneous character in both DCT and CDCT treatments compared to CHT treatment.

X-ray diffraction (XRD) analysis was conducted to identify phase constituents and assess crystal structure changes resulting from the various heat treatments. As shown in Fig. 5a, the diffraction patterns

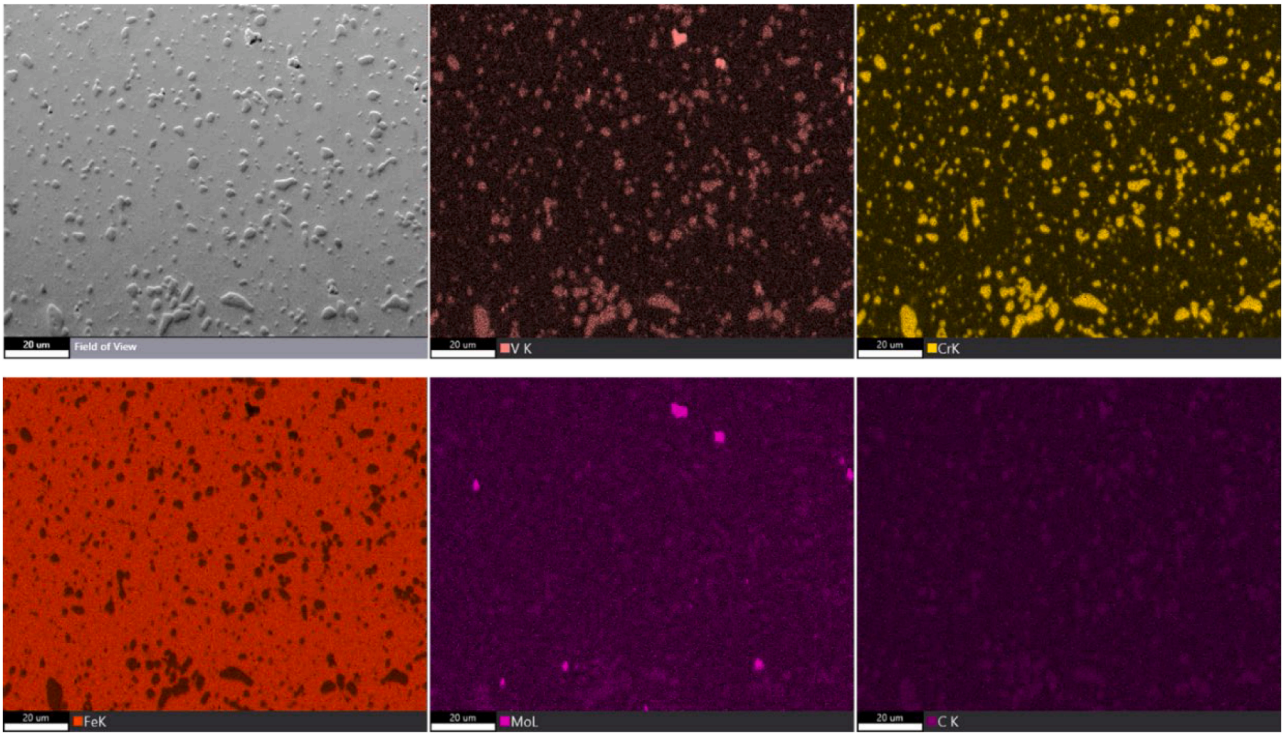

Fig. 4. Electron microscopic image and corresponding elemental maps of representative sample (CHT) acquired from EDS.

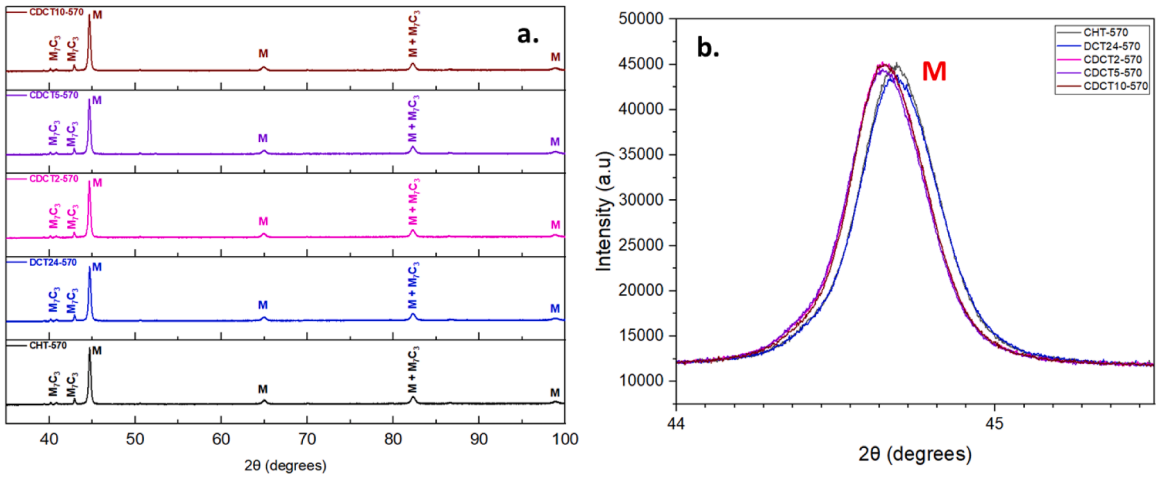

Fig. 5. XRD patterns of samples treated by different heat treatments. a: all diffraction peaks, b: reflection of Martensite peak at 2θ (≈ 45°).

primarily indicate the presence of martensite and carbides, with no detectable retained austenite. Furthermore, Fig. 5b reveals a shift in the martensite (M) diffraction peak towards lower angles in the sequence CHT to DCT24 to CDCT. According to Bragg's Law as shown in Eq. (2) and (3), this shift indicates an increase in the martensite lattice parameter, likely resulting from microstructural modifications such as lattice refinement or stress relaxation, dislocation density, or the introduction of crystal defects. Therefore, CDCT promotes greater changes in the state of martensite compared to the other treatments, which can contribute to improvements in both strength and toughness. In XRD analysis, clear peak shifting was observed, attributed to changes in residual stress and lattice parameters, while peak broadening was not observed. This could be because the dominant microstructural changes induced by CDCT under the specific experimental conditions primarily influenced the lattice strain and residual stresses (reflected in peak shifts) rather than causing significant changes in crystallite size reduction or introducing substantial micro-strain that would typically manifest as peak broadening.

$$2d\sin\theta = n\lambda \tag{2}$$

$$d = \frac{a}{\sqrt{h^2 + k^2 + l^2}} \tag{3}$$

For quantitative analysis of carbide distribution, twenty randomly selected backscattered electron (BSE) images were employed. Image-J software was utilized to assess the distribution based on the size of individual carbide particles. Fig. 6 presents a representative microstructure alongside the calculations employed to determine the mean particle count and size distribution of PCs, SCs, and SSCs for the various heat treatment conditions. The corresponding Image-J particle analysis is also included in the figure.

Fig. 6 presents the quantitative analysis of carbide size and distribution following various heat treatment conditions. The bar charts reveal a comparable distribution of PCs and SCs across CHT, DCT, and CDCT samples. This similarity can be attributed to the identical hardening parameters employed for all treatments. All the samples underwent identical hardening conditions, specifically an austenitization treatment at 1000 °C for 30 min. the formation and distribution of both PCs and SCs are strongly influenced by the austenitizing conditions, as these dictate the solubility limits of alloying elements and the subsequent nucleation and growth kinetics of carbides upon cooling. Since the

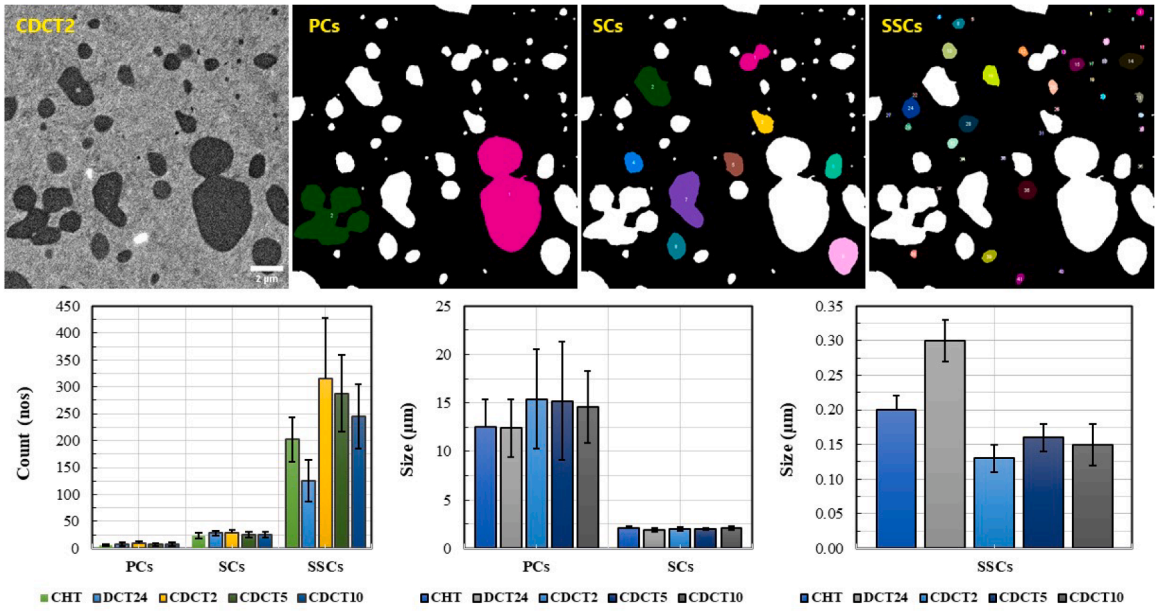

Fig. 6. BSE Microstructure of CDCT2 sample and corresponding Image-J analysis of carbides for their count and sizes.

hardening process was identical for all the treatments, it is expected that the carbide density and distribution of PCs and SCs would be similar, regardless of any subsequent modifications such as cryogenic treatments. However, a significant variation is observed in the size and distribution of SSCs.

CDCT treatment resulted in a substantial reduction in SSC size compared to CHT and DCT, with a noticeably higher fraction of particles falling within the submicron range. Notably, the count of SSCs increased with cyclic treatments, with CDCT2 samples exhibiting the highest number. Conversely, the size of SSCs decreased for all CDCT specimens. For example, the average size of SSCs in CDCT2, CDCT5, and CDCT10 treatments were 0.13 μm, 0.16 μm, and 0.15 μm, respectively, compared to 0.20 μm for CHT and 0.30 μm for DCT. These observations suggest a more refined microstructure and a more favorable distribution of carbides associated with CDCT treatments compared to the other two methods.

The refinement of microstructure [20,21] and the associated enhancement of finely dispersed carbides following deep cryogenic treatment have been consistently documented by various researches across diverse tool and die steels. For instance, Hadi et al. observed a significant increase in the volume fraction of submicron-sized carbides with an average diameter $<1^{\mu m}$ within the microstructure of AISI D2 steel when subjected to DCT [40]. Similar findings were also reported by other studies investigating the effects of DCT on various hot work [41] and high-speed steels [24]. These current findings collectively strengthen the notion that CDCT treatment is a viable technique to achieve a further refined microstructure with a potentially superior carbide distribution than CHT and DCT.

3.2. Hardness

Fig. 7 depicts the effect of various heat treatments on the mean macro- (bulk) and micro-hardness (tempered martensite matrix) of AISI D2 steel. Macro hardness measurements were conducted on nine samples, with each receiving at least twelve indentations to ensure a reliable average value. Microhardness was evaluated on three samples per condition, with at least six indentations performed on each sample. The results indicate no statistically significant differences in bulk hardness between D2 steel samples across all treatment groups, with values ranging from 47.5 HRC to 48 HRC. This is because microhardness, measured under higher loads, reflects the bulk material properties and is less sensitive to localized variations. Conversely, the microhardness (HV0.1) of specimens subjected to DCT24, CDCT2, CDCT5, and CDCT10 treatments exhibited higher values compared to the CHT group. The CHT specimen displayed a microhardness of 523 $HV_{0.1}$, whereas the DCT24, CDCT2, CDCT5, and CDCT10 specimens exhibited values of 554, 540, 559, and 539 HV0.1, respectively. Particularly, CDCT5 treatment yielded the highest microhardness among all groups and the magnitude of improvement in microhardness is around 6 % when compared to CHT. This underscores that CDCT-induced hardening and surface effects are better captured by microhardness due to its sensitivity to localized variations.

The influence of cryogenic treatment on the hardness of tool steels is predominantly governed by martensitic transformation rather than the carbide precipitation [19,35–37,42]. Cryogenic treatment promotes the transformation of retained austenite to martensite, leading to a significant increase in hardness, particularly observed in cold-work tool steels with high carbon content subjected to low-temperature tempering [38,39]. Conversely, high-temperature tempering treatments following cryogenic treatment can lead to decrease in hardness compared to conventional treatment [36,38,40,43–45]. This phenomenon is attributed to the loss of secondary hardening peak due to minimal or no retained austenite and potentially lower carbon content in the martensitic matrix due to enhanced carbide precipitation associated with cryogenic treatment, negating the beneficial effects of martensite formation [47,48]. Collectively, these opposing effects contribute to negligible changes in macro hardness. Current findings on the improvement of microhardness with deep cryogenic treatment and cyclic deep cryogenic treatments align with previous reports [49]. However, the extent of this improvement appears to be contingent on the specific cryogenic parameters employed.

3.3. Fracture toughness (K_{IC})

Fig. 8 represents the fracture toughness (K_{IC}) values of D2 steel after different heat treatment conditions. As depicted both DCT and CDCT treatments enhanced the K_{IC} values compared to CHT specimens. However, the magnitude of improvement varied across the different treatment groups. For instance, DCT24 treatment exhibited a 13 % increase in K_{IC} compared to CHT, while CDCT2, CDCT5, and CDCT10 treatments yielded improvements of 68 %, 5 %, and 9 %, respectively. Notably, CDCT2 specimen displayed the highest K_{IC} value amongst all the treated groups. This observation aligns with previous research on the impact of cryogenic treatments on tool and die steels. For instance, Yarasu et al. [50] reported enhanced fracture toughness after high-temperature tempering with cryogenic treatment, whereas a detrimental effect was observed at low tempering temperatures. Similarly, Das et al. [46] studied the effect of cryogenic treatment on the hardness and fracture toughness of D2 steel at low tempering temperatures. They documented an increase in hardness but a decrease in

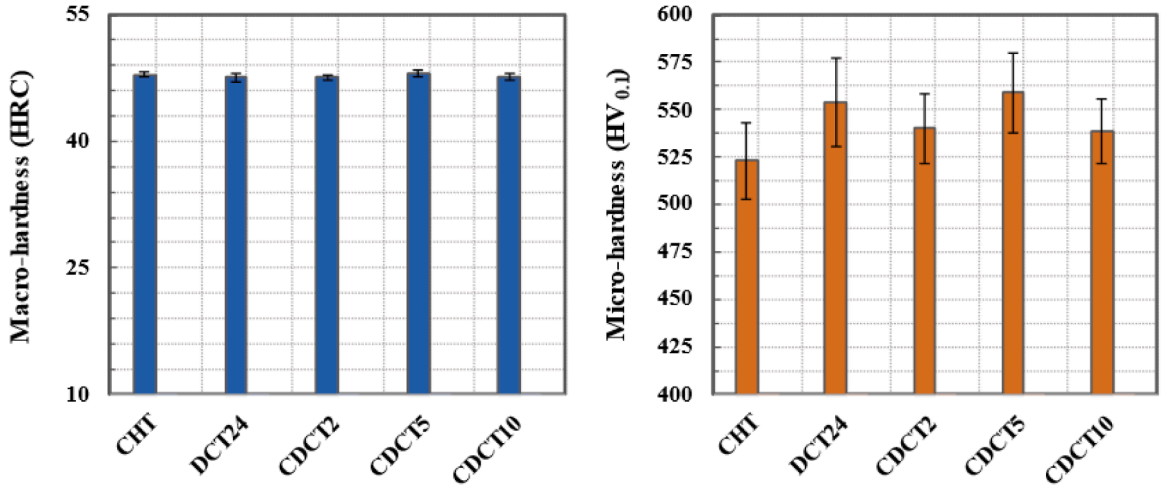

Fig. 7. Macro and Micro hardness of AISI D2 steel after different heat treatments.

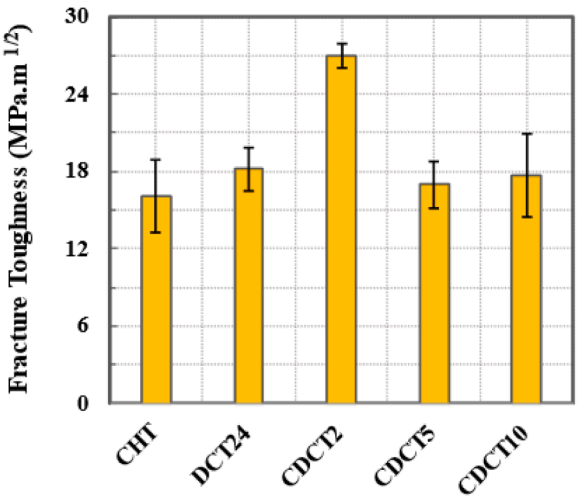

Fig. 8. Fracture toughness of AISI D2 steel after different heat treatments.

fracture toughness subjected to cryogenic treatment compared to CHT.

Furthermore, to elucidate the micro-mechanisms governing fracture behavior and establish a correlation between fracture toughness and developed microstructures, representative samples from each treatment group were examined using scanning electron microscopy (SEM). As illustrated in Fig. 9, the typical fracture surface revealed a combination of cleavage facets and microcracks indicative of brittle fracture originating from primary carbides (squares marked in yellow color), alongside micro-voids (circles marked in green color) associated with localized deformation within the tempered martensite matrix.

This morphology without any obvious differences was consistent across all specimen types, suggesting that micro-voids likely originated from the decohesion of secondary carbides. Notably, unlike primary carbides, no instances of secondary carbide cracking were observed on any fracture surfaces. However, the observed variations in K_{IC} values suggest an underlying difference in fracture resistance across the heat-treated samples, which could not be fully resolved at the microscopic level. While these variations were not readily discernible at the microscopic level, further investigations using transmission electron microscopy (TEM) coupled with energy-dispersive X-ray spectroscopy (EDS) were undertaken to gain insights into the structure-property relationships at the atomic scale.

Furthermore, Fig. 10 illustrates the impact of various heat treatments on the distribution of residual stress within D2 tool steel samples. CHT resulted in tensile residual stresses ranging from 405 to 285 MPa at the surface, with Von Mises stresses of 360 MPa. In contrast, DCT24 significantly reduced tensile stresses at the surface, achieving values approximately 69 % lower than those observed in CHT, ranging from 105 to 80 MPa, with Von Mises stresses of 155 MPa. Both CDCT5 and CDCT10 showed residual stress results similar to the DCT24 treatment. On the other hand, CDCT2 treatment produced compressive residual stresses at the surface, ranging from −60 to −65 MPa, with Von Mises stresses of ~80 MPa.

These results indicate that CHT induces substantial surface tensile stresses, while both DCT and CDCT generally lead to lower stresses, either tensile or compressive. This trend correlates with the observed fracture toughness values. Higher tensile residual stresses are generally detrimental to fracture toughness. The CHT sample, with its high tensile stresses, exhibited a fracture toughness of 16.1 MPa.$m^{-1/2}$. The DCT24 sample, with reduced tensile stresses, showed a 13 % improvement in fracture toughness (18.2 MPa.$m^{-1/2}$). CDCT5 and CDCT10 exhibit residual stress distributions similar to DCT24, leading to comparable increases in fracture toughness, with improvements of 5 % and 9 %, respectively, over the CHT sample. Notably, CDCT2, which induced surface compressive stresses, demonstrated a substantial 68 % increase in fracture toughness (27 MPa.$m^{-1/2}$). This treatment also slightly reduces core tensile stresses from 51 MPa to 15 MPa.

3.4. TEM characterization

High-angle annular dark (HAADF) and bright field (BF) scanning transmission electron microscopy (STEM) along with conventional TEM imaging coupled with EDS analysis was employed to examine the microstructural changes in D2 steel subjected to different treatments. As shown in Fig. 11, the TEM microstructure of the CDCT2 specimen

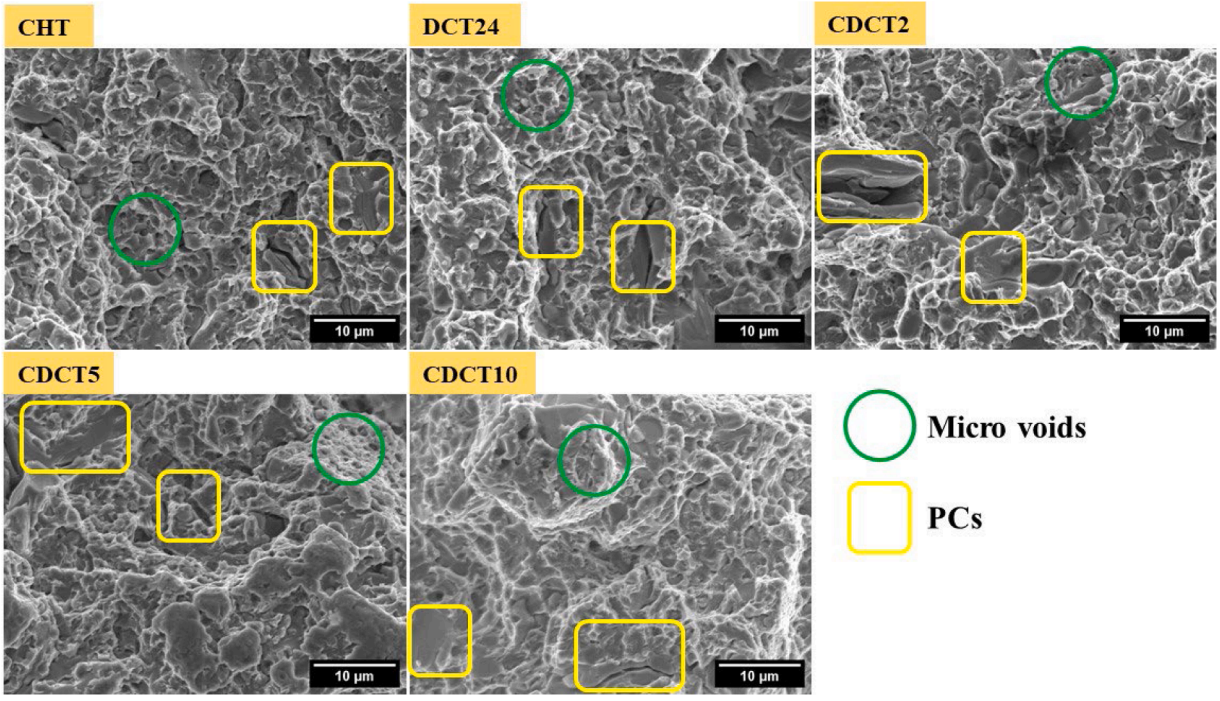

Fig. 9. Representative SEM fractography of developed fracture surfaces illustrating micro mechanisms of fracture.

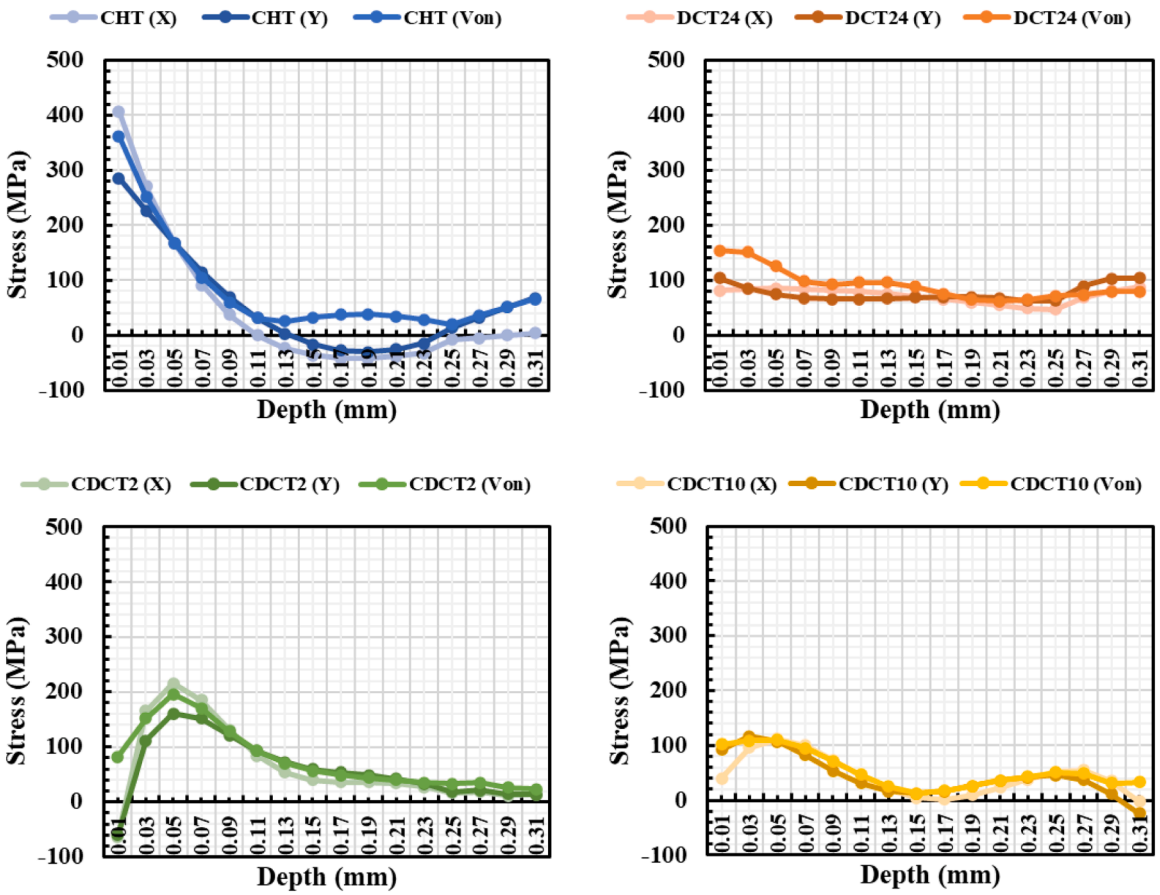

Fig. 10. Residual stresses distribution of different samples measured using IHD.

revealed a microstructure characteristic of fine tempered martensite. A high density of crystal defects dominates this microstructure, which includes stacking faults, twinned regions, dislocations, and a significant quantity of precipitates dispersed throughout the matrix. Notably, the martensitic matrix exhibits extensive decoration by these fine precipitates and crystal defects (twins and dislocations).

One of the significant findings in CDCT2-treated samples was the formation of extremely fine Cr precipitates, typically <150 nm in size (refer Fig. 6 for quantification of carbides). Additionally, Fig. 12 shows the TEM image and corresponding EDS maps for the distribution of Cr precipitates in a Fe-matrix for all three samples.

As shown in the TEM image, the density of fine Cr precipitates is observed to be higher in the CDCT2 sample in comparison with the CHT and DCT24 samples. These observations are in agreement with the quantification of carbides as detailed in Fig. 6. Moreover, the fine size of the Cr precipitates in CDCT2 samples suggests a more uniform and controlled precipitation process during the repeated cryogenic cycles.

Another distinct feature of DCT24 and CDCT2 samples is the refinement of martensite. For instance, both DCT24 and CDCT2 treatments resulted in the refinement of martensite having a mosaic-like structure (enlarged microstructure pointed by red arrow), as shown in Fig. 13. Moreover, the refinement of martensite is higher in CDCT2 treatment in comparison with DCT24. Whereas the CHT treated samples showed coarse martensite with no evidence of refinement.

Fine twins are another characteristic that is different between the treatments. Fig. 14 shows the stacking faults, or nanotwins, observed within the martensite lath. High-density network of stacking faults or nanotwins, as pointed by the arrows in Fig. 14 (enlarged image), is observed in both DCT24 and CDCT2 samples. The presence of crystal defects especially the staking faults and twins are confirmed by STEM investigation as shown in Fig. 15. These staking faults and nanotwins can strengthen the material by blocking the dislocation moment; hence, a high density of stacking faults or nanotwins in the CDCT2 sample can lead to more effective strengthening. It should be noted that these highly dense stacking faults were not observed in the CHT sample.

Furthermore, Fig. 16 compares and highlights the dislocations of all three samples. From the figure, it is observed that the microstructures of both DCT24 and CDCT2 samples have many dislocations compared to the microstructure of the CHT sample. It should be noted that these dislocations are decorated within the martensite domain as well as in the matrix. Therefore, based on the TEM observations, it can be concluded that, in comparison to conventional treatment and deep cryogenic treatment after 24 hours, CDCT2 samples showed a higher number of small secondary carbides, extensive Cr precipitation, and an increased number of crystal defects such as dislocations, stacking faults, or nanotwins, as well as refined tempered martensite.

The findings presented here are consistent with observations reported by other researches. The influence of deep cryogenic treatment (DCT) and tempering on the martensitic microstructure has been extensively studied in various tool steels. For instance, Li et al. [51] investigated the microstructure of a newly developed cold work die steel after DCT, reporting the presence of a twinned martensitic matrix along with enhanced precipitation of nano-sized carbides following tempering. Similarly, Durica et al. [52] recently documented an increased density of crystal defects, such as twins and dislocations, within the martensite of Vanadis 6 ledeburitic cold-work tool steel subjected to DCT.

As documented in previous studies [30,33,34,38], DCT generally refines and increases the number and population density of fine carbides within various tool steels. This process also promotes a more uniform carbide distribution through a categorization of the originally small secondary carbides. TEM micrographs from these studies have shown

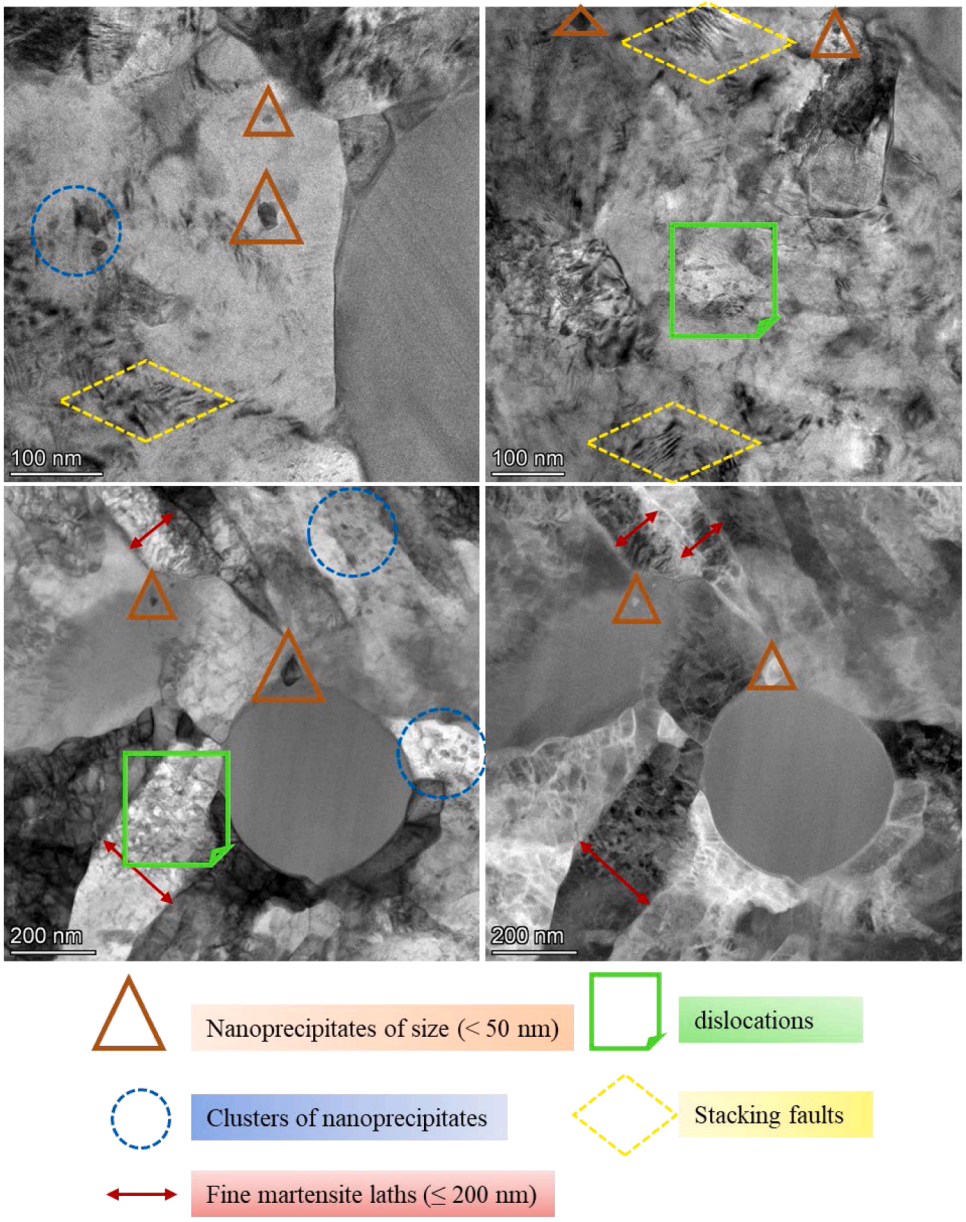

Fig. 11. TEM microstructures of CDCT2 sample: a & b) TEM images, c & d) high-angle annular bright-and dark field images.

the formation of not only nanosized carbides (ranging from 100 nm to <1 μm) but also a population of even smaller, newly formed precipitates (< 50 nm) within the martensite. These newly formed precipitates contribute to an overall increase in carbide content and a more homogenized carbide distribution following the DCT treatment. The results of the current investigation were comparable. For example, the martensite domains exhibit the development of nano-sized precipitates (< 50 nm) and fine carbides (<1 μm) in both DCT and CDCT treatments. In contrast to CHT and DCT24 treatments, CDCT2 treatment increased the precipitation of nanosized carbides <50 nm, and produced very fine carbides.

The presented TEM investigations reveal an enrichment of chromium within the newly formed nano-precipitates dispersed throughout the matrix after cyclic deep cryogenic treatment after 2-cycles. Notably, the tempered martensite phase (laths) exhibits a higher concentration of these chromium-rich nano-precipitates compared to other regions. Additionally, cyclic deep cryogenic treatment further refines the martensite laths and TEM observations of the CDCT2-treated sample reveal lath sizes below 200 nm. Moreover, the refined martensite matrix and laths of CDCT2 sample exhibits extensive decoration of crystal defects such as dislocations and stacking faults or nanotwins. Cycling DCT seems to provide additional activation energy for intensified nanotwin formation [53]. This suggests that cyclic treatment, which involves, repeated application of stress or thermal cycles, could indeed provide the necessary activation energy to enhance nanotwin formation. Therefore, the synergistic effect of nano-precipitate formation and the increased density of crystal defects within the martensite (dislocations, twins) are suggested to be the primary contributors to the enhanced mechanical properties, particularly the observed improvement in fracture toughness, following cyclic deep cryogenic treatment, especially after two cycles. These findings suggest that CDCT, particularly with a two-cycle regime, offers a promising approach to enhance the fracture toughness of AISI D2 cold-work tool steel without compromising the hardness in the given processed condition while potentially reducing the overall processing time of traditional DCT treatment.

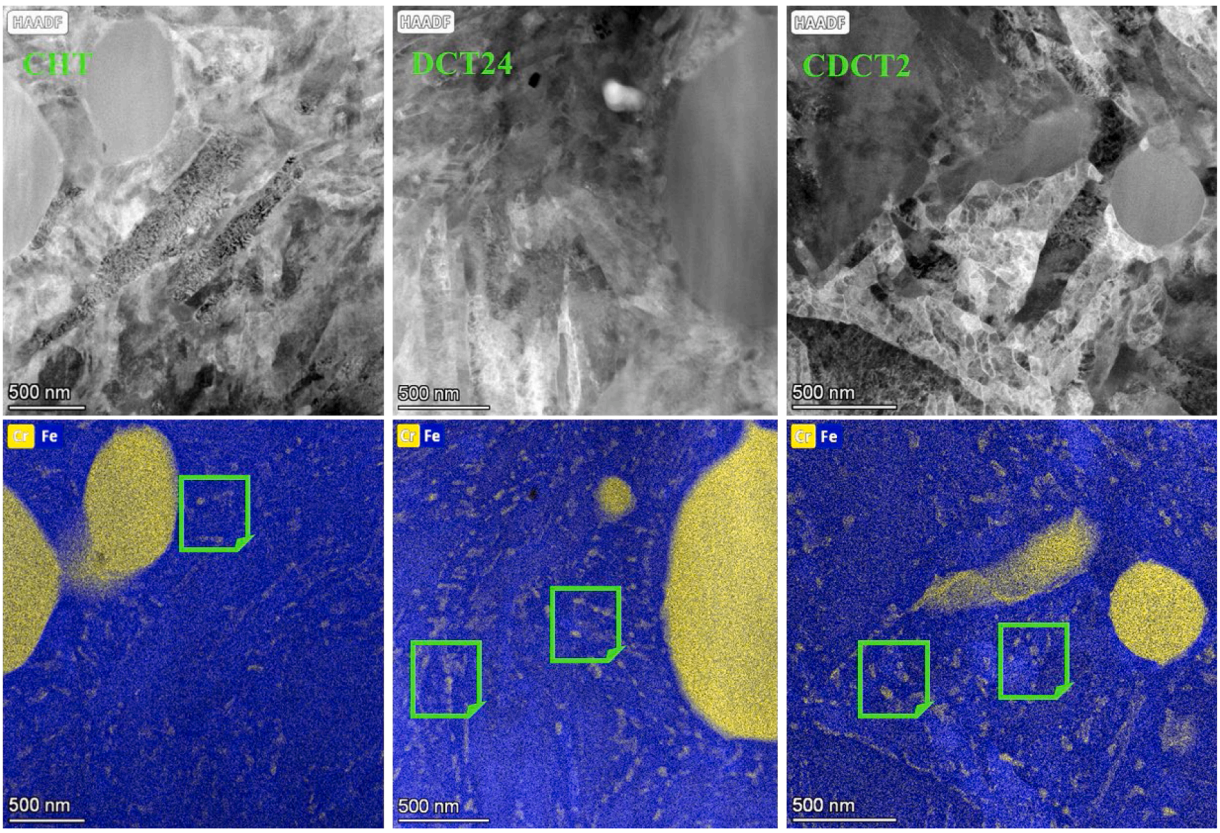

Fig. 12. Comparative TEM microstructures of different samples showing varying distribution of fine Cr precipitates.

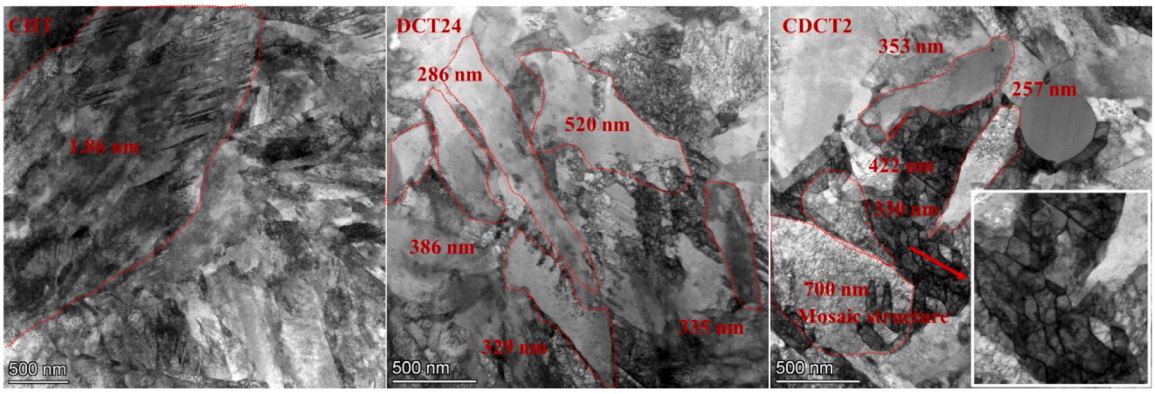

Fig. 13. Comparative TEM microstructures of different samples showing varying state of tempered martensite.

4. Conclusions

This investigation explored the impact of cyclic deep cryogenic treatment (CDCT) on the mechanical properties of AISI D2 cold-work tool steel. CDCT regimes with 2, 5, and 10 cycles were compared to conventional heat treatment (CHT) and deep cryogenic treatment (DCT). Based on the obtained results, the following conclusions can be drawn:

- Following high-temperature tempering, all treatment groups exhibited comparable macro-hardness values. However, CDCT displayed a statistically significant increase (about 6 %) in micro-hardness compared to CHT.
- Compared to other treatments, CDCT2 produced lower and more stable tensile stresses with depth and compressive stresses near the surface.
- Both DCT and CDCT demonstrably improved the properties of D2 steel, particularly regarding fracture toughness.
- CDCT, specifically with two cycles (CDCT2), yielded a remarkable 68 % enhancement in fracture toughness relative to CHT. This finding highlights the potential of CDCT to achieve superior performance with a reduced treatment duration.
- Fractographic analysis revealed a consistent fracture mode across all treatment groups, characterized by the presence of cleavage facets, micro-cracks, and micro-voids.
- The superior fracture toughness observed in CDCT2 samples can be attributed to the presence of nanoscale precipitates and refined

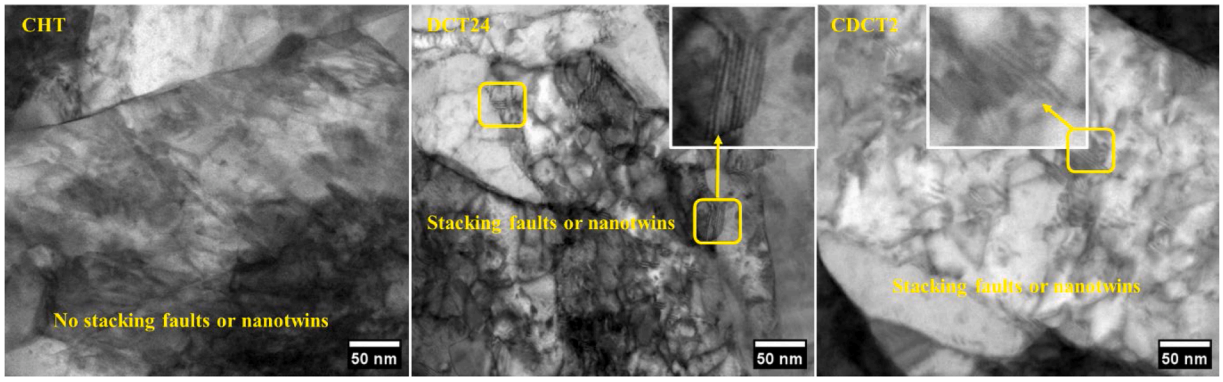

Fig. 14. Comparative TEM microstructures of different samples showing varying state of crystal defects (stacking faults or nanotwins).

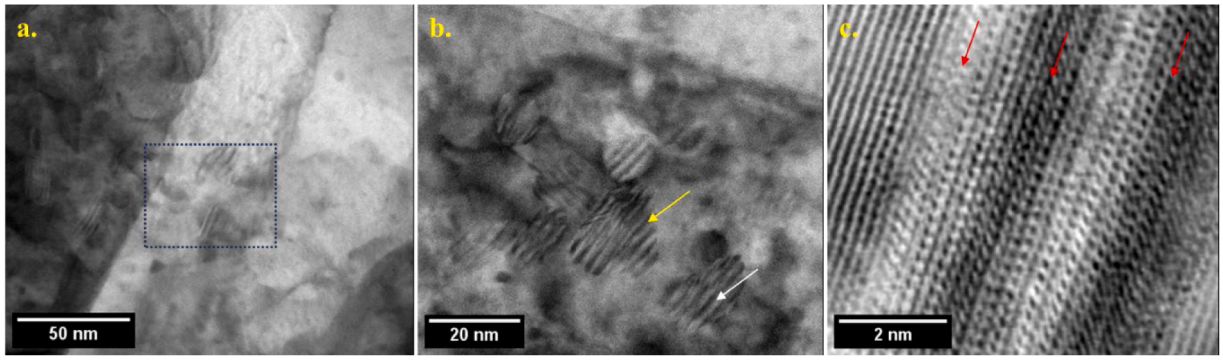

Fig. 15. CDCT2 sample, STEM BF images corresponding to (a.) a region with high presence of defects, especially stacking faults and twins, (b.) marked area showing typical contrast features indicating (c.) stacking faults and twins as signaled by the arrows.

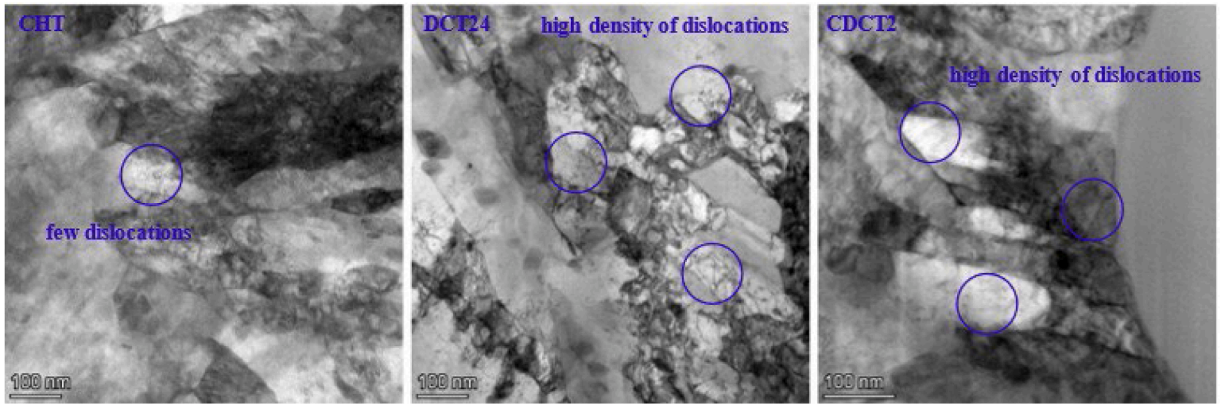

Fig. 16. Comparative TEM microstructures of different samples showing varying state of crystal defects (dislocations).

martensite laths, increased stacking faults, nano-twins within the martensite, and a higher dislocation density.

CRediT authorship contribution statement

Venu Yarasu: Writing – original draft, Visualization, Validation, Methodology, Investigation, Formal analysis, Data curation, Conceptualization. **Bojan Podgornik:** Writing – review & editing, Validation, Supervision, Resources, Project administration, Funding acquisition, Conceptualization. **Barbara Setina Batic:** Validation, Investigation, Formal analysis. **Marko Sedlacek:** Writing – review & editing, Resources. **Črtomir Donik:** Validation, Investigation. **Francisco Ruiz-Zepeda:** Validation, Investigation, Formal analysis.

Declaration of competing interest

The authors declare that they have no known competing financial interests or personal relationships that could have appeared to influence the work reported in this paper.

Acknowledgements

The authors acknowledge the financial support from the Slovenian Research and Innovation Agency (research core funding no P2-0050). The authors also acknowledge the technical and scientific staff assistance of Institute of Metals and Technology, Slovenia.

References

[1] C. Berger, H. Scheerer, J. Ellermeier, Modern materials for forming and cutting tools – overview, Mater. Werkst. 41 (2010) 5–16, https://doi.org/10.1002/mawe.200900529.

[2] S. Jhavar, C.P. Paul, N.K. Jain, Causes of failure and repairing options for dies and molds: a review, Eng. Fail. Anal. 34 (2013) 519–535, https://doi.org/10.1016/j.engfailanal.2013.09.006.

[3] A. Rizzo, S. Goel, M.L. Grilli, R. Iglesias, L. Jaworska, V. Lapkovskis, P. Novak, B. O. Postolnyi, D. Valerini, The critical raw materials in cutting tools for machining applications: a review, Mater. (Basel) 13 (2020) 1377, https://doi.org/10.3390/ma13061377.

[4] S. Elghazaly, Innovations in cold work tool steels- research and development, Int. J. Mater. Technol. Innov. 3 (2023) 64–73, https://doi.org/10.21608/ijmti.2023.198375.1080.

[5] D. Toboła, W. Brostow, K. Czechowski, P. Rusek, Improvement of wear resistance of some cold working tool steels, Wear 382–383 (2017) 29–39, https://doi.org/10.1016/j.wear.2017.03.023.

[6] B. Skela, M. Sedlaček, F. Kafexhiu, B. Podgornik, Influence of microstructure and mechanical properties of hot-work tool steel on wear resistance subjected to high-stress wear conditions, Tribol. Lett. 68 (2020) 58, https://doi.org/10.1007/s11249-020-01300-1.

[7] G.Y. Baek, G.Y. Shin, K.Y. Lee, D.S. Shim, Mechanical properties of tool steels with high wear resistance via directed energy deposition, Metal. (Basel) 9 (2019) 282, https://doi.org/10.3390/met9030282.

[8] G.S. Goindi, P. Sarkar, Dry machining: a step towards sustainable machining – challenges and future directions, J. Clean. Prod. 165 (2017) 1557–1571, https://doi.org/10.1016/j.jclepro.2017.07.235.

[9] J.C. Najmon, S. Raeisi, A. Tovar, Review of additive manufacturing technologies and applications in the aerospace industry, in: Addit. Manuf. Aerosp. Ind., Elsevier, 2019, pp. 7–31, https://doi.org/10.1016/B978-0-12-814062-8.00002-9.

[10] G. Saha, K. Valtonen, A. Saastamoinen, P. Peura, V.-T. Kuokkala, Impact-abrasive and abrasive wear behavior of low carbon steels with a range of hardness-toughness properties, Wear 450–451 (2020) 203263, https://doi.org/10.1016/j.wear.2020.203263.

[11] A. Hosseini, H.A. Kishawy, Cutting tool materials and tool wear, in: J.P. Davim (Ed.), Mach. Titan. Alloys, Springer Berlin Heidelberg, Berlin, Heidelberg, 2014, pp. 31–56, https://doi.org/10.1007/978-3-662-43902-9_2.

[12] R. Besler, M. Bauer, K.P. Furlan, A.N. Klein, R. Janssen, Effect of processing route on the microstructure and mechanical properties of hot work tool steel, Mater. Res. 20 (2017) 1518–1524, https://doi.org/10.1590/1980-5373-mr-2016-0726.

[13] F. Großwendt, A. Röttger, A. Strauch, A. Chehreh, V. Uhlenwinkel, R. Fechte-Heinen, F. Walther, S. Weber, W. Theisen, Additive manufacturing of a carbon-martensitic hot-work tool steel using a powder mixture – Microstructure, post-processing, mechanical properties, Mater. Sci. Eng. A 827 (2021) 142038, https://doi.org/10.1016/j.msea.2021.142038.

[14] M. Momeni, Effects of heat treatment on mechanical properties of modified cast AISI D3 tool steel, Mater. Des. 54 (2014) 742–747.

[15] B. Podgornik, G. Puš, B. Žužek, V. Leskovšek, M. Godec, Heat treatment optimization and properties correlation for H11-type hot-work tool steel, Metall. Mater. Trans. A 49 (2018) 455–462, https://doi.org/10.1007/s11661-017-4430-1.

[16] D. Lesyk, S. Martinez, B. Mordyuk, V. Dzhemelinskyi, O. Danyleiko, Effects of the combined laser-ultrasonic surface hardening induced microstructure and phase State on mechanical properties of AISI D2 tool steel, in: V. Ivanov, J. Trojanowska, J. Machado, O. Liaposhchenko, J. Zajac, I. Pavlenko, M. Edl, D. Perakovic (Eds.), Adv. Des. Simul. Manuf. II, Springer International Publishing, Cham, 2020, pp. 188–198, https://doi.org/10.1007/978-3-030-22365-6_19.

[17] S.M.T. Omar, K.P. Plucknett, The influence of DED process parameters and heat-treatment cycle on the microstructure and hardness of AISI D2 tool steel, J. Manuf. Process. 81 (2022) 655–671, https://doi.org/10.1016/j.jmapro.2022.06.069.

[18] S. Kumar, N.K. Khedkar, B. Jagtap, T.P. Singh, The effects of cryogenic treatment on cutting tools, IOP Conf. Ser. Mater. Sci. Eng 225 (2017) 012104, https://doi.org/10.1088/1757-899X/225/1/012104.

[19] A. Akhbarizadeh, A. Shafyei, M.A. Golozar, Effects of cryogenic treatment on wear behavior of D6 tool steel, Mater. Des. 30 (2009) 3259–3264, https://doi.org/10.1016/j.matdes.2008.11.016.

[20] M.A. Essam, A.Y. Shash, M.K. El-Fawakhry, E. El-Kashif, H. Megahed, Effect of deep cryogenic treatment on wear behavior of cold work tool steel, Metal. (Basel) 13 (2023) 382, https://doi.org/10.3390/met13020382.

[21] M.A. Essam, A.Y. Shash, M.K. El-Fawakhry, E. El-Kashif, H. Megahed, Influence of micro-alloying elements and deep cryogenic treatment on microstructure and mechanical properties of S5 cold work shock resisting tool steel, Result. Mater. 17 (2023) 100374, https://doi.org/10.1016/j.rinma.2023.100374.

[22] D. Das, A.K. Dutta, K.K. Ray, Influence of varied cryotreatment on the wear behavior of AISI D2 steel, Wear 266 (2009) 297–309, https://doi.org/10.1016/j.wear.2008.07.001.

[23] P. Jurči, J. Ďurica, I. Dlouhý, J. Horník, R. Planieta, D. Kralovič, Application of −140°C sub-zero treatment for Cr-V ledeburitic steel service performance improvement, Metall. Mater. Trans. A 50 (2019) 2413–2434, https://doi.org/10.1007/s11661-019-05180-6.

[24] G. Xu, P. Huang, Z. Feng, Z. Wei, G. Zu, Effect of deep cryogenic time on martensite multi-level microstructures and mechanical properties in AISI M35 high-speed steel, Mater. (Basel) 15 (2022) 6618, https://doi.org/10.3390/ma15196618.

[25] M. Zhang, K. Li, X. Shi, L. Guo, L. Feng, T. Duan, Influence of cryogenic thermal cycling treatment on the thermophysical properties of carbon/carbon composites between room temperature and 1900°C, J. Mater. Sci. Technol. 34 (2018) 409–415, https://doi.org/10.1016/j.jmst.2017.03.001.

[26] R. Gecu, Combined effects of cryogenic treatment and tempering on microstructural and tribological features of AISI H13 steel, Mater. Chem. Phys. 292 (2022) 126802, https://doi.org/10.1016/j.matchemphys.2022.126802.

[27] A. Boztepe, R. Gecu, Influence of cryogenic treatment and tempering temperature on microstructural evolution and dry sliding wear behavior of AISI D3 cold-work tool steel, J. Tribol. 147 (2025) 064201, https://doi.org/10.1115/1.4067045.

[28] A. Boztepe, R. Gecü, Achieving synergistic improvement on wear performance of D3 cold-work steel by modifying the number and order of deep cryogenic and tempering treatments, Tribol. Trans. (2025) 1–14, https://doi.org/10.1080/10402004.2025.2462566.

[29] H. Li, W. Zhao, T. Chen, Y. Huang, J. Sun, P. Zhu, Y. Lu, A.H.W. Ngan, D. Wei, Q. Du, Y. Zou, Beneficial effects of deep cryogenic treatment on mechanical properties of additively manufactured high entropy alloy: cyclic vs single cryogenic cooling, J. Mater. Sci. Technol. 115 (2022) 40–51, https://doi.org/10.1016/j.jmst.2021.11.022.

[30] J.W. Lv, F.L. Wang, D.W. Yin, S. Zhang, Z.Q. Cai, Z.L. Shi, M.Z. Ma, X.Y. Zhang, Effect of deep cryogenic cycling treatment on the microstructure and mechanical properties of Ti-based bulk metallic glass, J. Alloy. Compd. 887 (2021) 161386, https://doi.org/10.1016/j.jallcom.2021.161386.

[31] R. Su, S. Ma, K. Wang, G. Li, Y. Qu, R. Li, Effect of cyclic deep cryogenic treatment on corrosion resistance of 7075 alloy, Met. Mater. Int. 28 (2022) 862–870, https://doi.org/10.1007/s12540-021-00975-y.

[32] H. Zhang, X. Yan, Q. Hou, Z. Chen, Effect of cyclic cryogenic treatment on wear resistance, impact toughness, and microstructure of 42CrMo steel and its optimization, Adv. Mater. Sci. Eng. 2021 (2021) 1–13, https://doi.org/10.1155/2021/8870282.

[33] Z. Wang, S. Shi, J. Yu, B. Li, Y. Li, X. Chen, Combining multiscale structure and TRIP effect to enhance room temperature tensile properties of 304 stainless steel by cryogenic cyclic plastic strengthening, Scr. Mater. 234 (2023) 115581, https://doi.org/10.1016/j.scriptamat.2023.115581.

[34] Z. Chen, L. Jing, Y. Gao, Y. Huang, J. Guo, X. Yan, Impact of cryogenic treatment process on the performance of 51CrV4 steel, Mater. (Basel) 16 (2023) 4399, https://doi.org/10.3390/ma16124399.

[35] B. Podgornik, B. Žužek, V. Leskovšek, Experimental evaluation of tool steel fracture toughness using circumferentially notched and precracked tension bar specimen, Mater. Perform. Charact. 3 (2014) 87–103, https://doi.org/10.1520/MPC20130045.

[36] ASM international, ASM handbook, ed., ASM international, Materials park (Ohio), 1991.

[37] S. Wei, Z. Tingshi, G. Daxing, L. Dunkang, L. Poliang, Q. Xiaoyun, Fracture toughness measurement by cylindrical specimen with ring-shaped crack, Eng. Fract. Mech. 16 (1982) 69–82, https://doi.org/10.1016/0013-7944(82)90036-4.

[38] D. Das, A.K. Dutta, V. Toppo, K.K. Ray, Effect of deep cryogenic treatment on the carbide precipitation and tribological behavior of D2 steel, Mater. Manuf. Process 22 (2007) 474–480, https://doi.org/10.1080/10426910701235934.

[39] M.F.C. Moscoso, F.D. Ramos, C.R. De Lima Lessa, P.H.C.P. Cunha, J.C. Toniolo, G. V.B. Lemos, Effects of cooling parameter and cryogenic treatment on microstructure and fracture toughness of AISI D2 tool steel, J. Mater. Eng. Perform. 29 (2020) 7929–7939, https://doi.org/10.1007/s11665-020-05285-9.

[40] H. Ghasemi-Nanesa, M. Jahazi, Simultaneous enhancement of strength and ductility in cryogenically treated AISI D2 tool steel, Mater. Sci. Eng. A 598 (2014) 413–419, https://doi.org/10.1016/j.msea.2014.01.065.

[41] Jalil Soleimany, H. Ghayour, K. Amini, F. Gharavi, The effect of deep cryogenic treatment on microstructure and wear behavior of H11 tool steel, Phys. Met. Metallogr. 120 (2019) 888–897, https://doi.org/10.1134/S0031918X19090035.

[42] D.N. Collins, J. Dormer, Classic contributions: cryogenic treatment deep cryogenic treatment of a D2 cold work tool steel, Int. Heat Treat. Surf. Eng. 2 (2008) 150–154, https://doi.org/10.1179/174951508X446376.

[43] P. Jurči, I. Dlouhý, J. Horník, P. Priknerová, Z. Mrštný, Relationships between the microstructure, hardness and fracture toughness of differently sub-zero treated tool steel, defect diffus, Forum Fam. Plan. West Hemisph. 395 (2019) 95–112, https://doi.org/10.4028/www.scientific.net/DDF.395.95.

[44] V. Yarasu, P. Jurci, J. Hornik, Enhancing tribological performance in PM Vanadis 6 steel through optimization of cryogenic and tempering treatment, Tribol. Int. 195 (2024) 109564, https://doi.org/10.1016/j.triboint.2024.109564.

[45] V. Yarasu, P. Jurci, P. Gogola, B. Podgornik, M. Sedlaček, Sliding wear behaviour of conventional and cryotreated PM Cr-V (Vanadis 6) ledeburitic tool steel, Wear 532–533 (2023) 205107, https://doi.org/10.1016/j.wear.2023.205107.

[46] D. Das, K.K. Ray, Structure–property correlation of sub-zero treated AISI D2 steel, Mater. Sci. Eng. A 541 (2012) 45–60, https://doi.org/10.1016/j.msea.2012.01.130.

[47] V. Yarasu, P. Jurci, J. Hornik, S. Krum, Optimization of cryogenic treatment to improve the tribological behavior of Vanadis 6 steel using the Taguchi and grey relation approach, J. Mater. Res. Technol. 18 (2022) 2945–2962, https://doi.org/10.1016/j.jmrt.2022.03.145.

[48] A. Ciski, Deep cryogenic treatment and tempering at different temperatures of HS6-5-2 high speed steel, Arch. Metall. Mater. (2018), https://doi.org/10.24425/122424.

[49] J.D. Darwin, D. Mohan Lal, G. Nagarajan, Optimization of cryogenic treatment to maximize the wear resistance of 18% Cr martensitic stainless steel by Taguchi method, J. Mater. Process. Technol. 195 (2008) 241–247, https://doi.org/10.1016/j.jmatprotec.2007.05.005.

[50] V. Yarasu, P. Jurci, J. Ptacinova, I. Dlouhy, J. Hornik, Effect of cryogenic treatments on hardness, fracture toughness, and wear properties of Vanadis 6 tool steel, Mater. (Basel) 17 (2024) 1688, https://doi.org/10.3390/ma17071688.
[51] S. Li, N. Min, J. Li, X. Wu, C. Li, L. Tang, Experimental verification of segregation of carbon and precipitation of carbides due to deep cryogenic treatment for tool steel by internal friction method, Mater. Sci. Eng. A 575 (2013) 51–60, https://doi.org/10.1016/j.msea.2013.03.070.
[52] J. Ďurica, J. Ptačinová, M. Dománková, L. Čaplovič, M. Čaplovičová, L. Hrušovská, V. Malovcová, P. Jurči, Changes in microstructure of ledeburitic tool steel due to vacuum austenitizing and quenching, sub-zero treatments at −140°C and tempering, Vacuum 170 (2019) 108977, https://doi.org/10.1016/j.vacuum.2019.108977.
[53] M. Villa, M.A.J. Somers, Thermally activated martensite formation in ferrous alloys, Scr. Mater. 142 (2018) 46–49, https://doi.org/10.1016/j.scriptamat.2017.08.024.